*Journal of Applied Electrochemistry* **31**: 677–683, 2001.



# Electrochemical characterization of Ni–P and Ni–Co–P amorphous alloy deposits obtained by electrodeposition

M.M.V. PARENTE[1,2], O.R. MATTOS[1]*, S.L. DÍAZ[1], P. LIMA NETO[2] and F.J. FABRI MIRANDA[3]
[1]*Laboratório de Corrosão Prof. Manoel de Castro, EE/PEMM/COPPE, Universidade Federal do Rio de Janeiro, Cx. Postal 68505, CEP 21945-970, Rio de Janeiro, RJ, Brazil*
[2]*Departamento de Química Analítica e Físico-Química, Universidade Federal do Ceará, CE, Brazil*
[3]*Centro de Pesquisa e Desenvolvimento da USIMINAS, Ipatinga, MG, Brazil*
*(*author for correspondence, e-mail: omattos@metalmat.ufri.br, fax: +55 21 290 6626)*

Received 14 August 2000; accepted in revised form 25 January 2001

*Key words:* alloy electrodeposition, amorphous alloys, impedance, Ni–Co–P alloy, Ni–P alloy

**Abstract**

Ni–P and Ni–Co–P amorphous alloy deposits were obtained by electrodeposition at 80 °C on carbon steel substrates. The influence of the electrolyte $Co^{2+}$ concentration and of applied current density was investigated. The corrosion behaviour of amorphous and crystalline deposits was evaluated by polarization curves and electrochemical impedance spectroscopy in NaCl 0.1 M solution at room temperature. Impedances were measured for samples under total immersion (free potential against time) and for polarized samples in predefined regions of the polarization curves. It was found that the alloy deposit composition is highly affected by the composition of the electrolyte but displays no significant dependence on applied current density. The results showed that the presence of Co on Ni–P amorphous alloys improves the deposit performance in the studied corrosive medium. It was also verified that the amorphous structure provides higher corrosion resistance to both Ni–P and Ni–Co–P alloys.

## 1. Introduction

Metal alloys with noncrystalline structure have attracted the interest of many researchers in the last two decades for their distinct mechanical and magnetic properties and especially, for their corrosion resistance [1]. These alloys can be produced by a variety of methods including electrodeposition. In particular, Ni–P alloys, as corrosion protective coatings, constitute one of the earliest industrial applications of amorphous metals [1, 2]. These alloys are widely used for corrosion protection in many corrosive environments such as the oil and gas industries, mining and chemical manufacture. Despite extensive research on this alloy, inconsistencies concerning the relationship between the electrodeposition parameters and the alloy composition still remain. Some investigations have reported that the highest P content is obtained at low overpotentials [1, 3] and at low Ni concentration in solution [1]. Contrary to this, Budniok et al. [4] showed that, with an increase in current density, the P content in the alloys is also increased, while Morikawa et al. [5] observed no significant dependence of P content on current density. Common points of agreement are also reported. For instance, it is generally accepted that an increase in P content is accompanied by a transition from a crystalline to an amorphous alloy structure [2, 3, 6–10], although the composition which separates crystalline from amorphous structures is not clearly defined.

Functional properties of Ni–P coatings are sensitive to their structural state and P content. Good corrosion resistance seems to result from high P content and the corresponding amorphous structure. Published data display controversial information concerning the corrosion characteristics of Ni–P alloys, especially about the nature of its anodic dissolution, ability to passivate and susceptibility to pitting [1–3, 8, 9, 11–14]. Some investigations have showed that amorphous Ni–P alloys do not passivate in acidic media [11–14] and display intense active dissolution [11]. Habazaki et al. [12] and Splinter et al. [13] concluded from XPS analysis that the active dissolution of Ni–P leads to accumulation of P on the surface as a result of selective dissolution of Ni during polarization. A $Ni_3(PO_4)_2$ film is then formed, acting as a barrier against the dissolution. In contrast, Carbajal et al. [1] observed passivation in basic, neutral saline and acid media followed by an increase in current with anodic potential. They suggested dissolution through the passive film and/or a change of oxidation state of the components. Diegle et al. [14] suggested that Ni–P alloy does not develop a classical passive film and proposed that the passivation process is controlled by the

formation and adsorption of hypophosphite anion, which forms a barrier layer between the alloy and the electrolyte. Transpassivity should result from oxidation of P from this film and is accompanied by stoichiometric alloy dissolution. A similar passivation mechanism was proposed for Co–P in acidic medium [15]. Bielinski et al. [11] postulated that the inhibition of P oxidation on amorphous Ni–P causes preferential dissolution of Ni and surface segregation of a P enriched Ni–P phase, which is more stable and acts as a barrier for further Ni dissolution. Lo et al. [9] showed by EIS measurements that increasing P content causes an increase in the Rt of Ni–P alloy deposits in NaCl solutions. The authors explained this behaviour in terms of passivity involving the adsorption of hypophosphite ions on the alloy surface. Królikowski et al. [2] showed that EIS diagrams obtained during anodic polarization of Ni–P deposits are strongly dependent on the structural state of the alloy.

The aim of the present work is to contribute to a better insight into the anodic behaviour of Ni–P alloys relative to their structural state. Another purpose is to evaluate the effects of alloying Co on the corrosion properties of Ni–P coatings. The influence of applied current density and electrolyte $Co^{2+}$ concentration on the composition of alloy deposits has been investigated. The corrosion behaviour of amorphous and crystalline deposits, obtained by heat treatment, was evaluated by polarization curves and electrochemical impedance spectroscopy in NaCl 0.1 M at room temperature.

## 2. Experimental details

Ni–P and Ni–Co–P alloy deposits were obtained by electrodeposition from solutions with the following composition: 174 g $l^{-1}$ $NiSO_4 \cdot 6\,H_2O$ + 47 g $l^{-1}$ $NiCl_2 \cdot 6\,H_2O$ + 5–15 g $l^{-1}$ $Na_2CO_3$ + 63 g $l^{-1}$ $NaH_2PO_2 \cdot H_2O$ + 51 g $l^{-1}$ $H_3PO_4$ and $X$ $CoSO_4 \cdot 6H_2O$ ($X = 0$, 50 and 100 g $l^{-1}$). Solutions were prepared from Merck pro-analysis grade chemicals and double-distilled water. The pH of the solutions was 2 at 80 °C. Electrodeposition was carried out under galvanostatic conditions for current densities of 30, 60, 90 and 120 mA $cm^{-2}$ at a temperature of 80 °C on mild steel substrates. Prior to electroplating, the substrates were mechanically polished with silicon carbide emery paper, degreased in a 1 M NaOH solution at 80 °C and then pickled in 20% HCl. During deposition, the bath was mildly stirred using a magnetic stirrer.

After electrodeposition, some samples were heat-treated at 500 °C [4] in a $N_2$ atmosphere for 1 h in order to change the deposit structure from amorphous to crystalline. The structures of alloy deposits were analysed by X-ray diffraction (XRD) and their chemical composition determined by atomic absorption, for Ni and Co, and by a colorimetric method, for P. The microstructure was characterized by scanning electron microscopy (SEM). The corrosion behaviour of the obtained coatings was investigated by electrochemical methods. Measurements were performed in 0.1 M NaCl, open to air and at room temperature in a conventional three-electrode cell. A platinum grid was used as counter electrode and a saturated calomel electrode as reference. All values of potential are given with respect to this latter electrode. Anodic polarization curves were obtained in potentiostatic mode. Impedances were measured for samples under total immersion (free potential against time) and for polarized samples at predefined regions of the polarization curves. In this last case, before starting the measurements, the samples were exposed to the applied potential for 1 h to reach a steady current value. The frequency range used was 40 kHz to 2 mHz, with an amplitude perturbation of 10 mV.

## 3. Results and discussion

Table 1 presents, as a function of applied current density, the results concerning the chemical analysis of alloy deposits obtained in solution without addition of $CoSO_4 \cdot 6H_20$ (NiP) and with addition of 50 g $l^{-1}$ (NiCoP50) and 100 g $l^{-1}$ (NiCoP100) of the Co salt. It should be noted that the composition of the Ni–P alloys shows no significant dependence on current density. The P content remains almost constant around 17 at %. The addition of $Co^{2+}$ to the electrolyte causes modifications of alloy composition. It was found that Co content increases with increasing current density and with increasing $Co^{2+}$ concentration in the electrolyte. However, the P content of Ni–Co–P alloys shows no clear dependence on solution composition.

The morphology of deposits also changes with solution composition. Figure 1 shows the micrographs of deposits obtained at 120 mA $cm^{-2}$ from (a) NiP, (b) NiCoP50 and (c) NiCoP100 solutions. It is possible to note that the morphology changes from granular, for the Ni–P alloy (Figure 1(a)), to columnar for the Ni–Co–P alloy deposits (Figures 1(b) and (c)). Indeed, this characteristic becomes more accentuated as the Co content increases from 26.2 at % (b) to 39.9 at % (c).

*Table 1.* Chemical composition of alloy deposits as a function of applied current density

| Solution | Applied current /mA $cm^{-2}$ | Ni /at % | Co /at % | P /at % |
|---|---|---|---|---|
| NiP | 30 | 82.4 | – | 17.6 |
| | 60 | 82.8 | – | 17.2 |
| | 90 | 80.5 | – | 19.5 |
| | 120 | 82.9 | – | 17.1 |
| NiCoP50 | 30 | 66.6 | 17.0 | 16.4 |
| | 60 | 53.3 | 26.2 | 20.5 |
| | 90 | 56.8 | 27.3 | 15.9 |
| | 120 | 59.8 | 26.2 | 14.0 |
| NiCoP100 | 30 | 55.2 | 26.3 | 18.5 |
| | 60 | 46.1 | 34.9 | 19.0 |
| | 90 | 50.0 | 35.5 | 14.5 |
| | 120 | 46.2 | 39.9 | 13.9 |

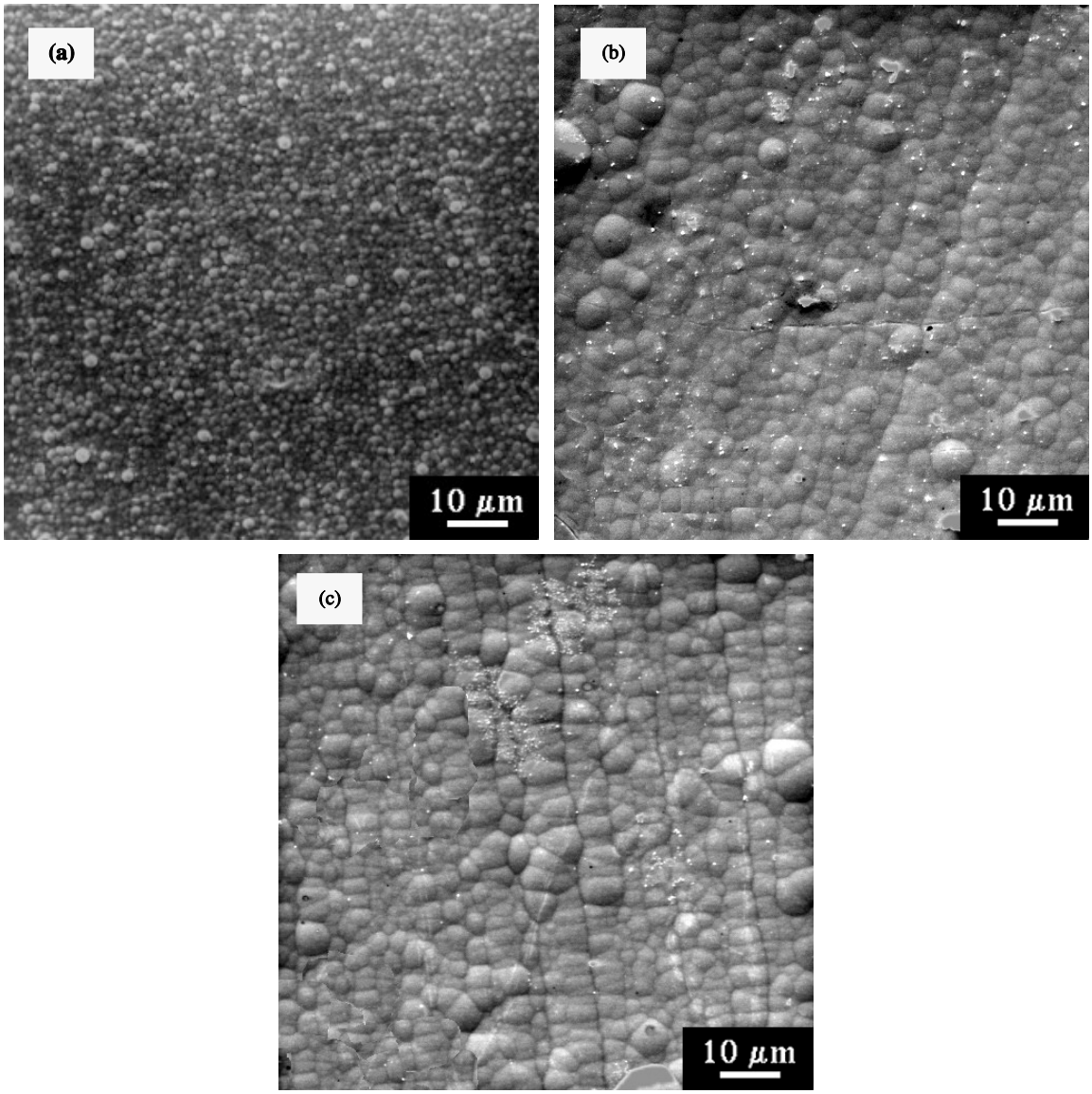


*Fig. 1.* Effects of solution composition on morphology of alloy deposits obtained at 120 mA $cm^{-2}$ from: (a) NiP, (b) NiCoP50 and (c) NiCoP100 solutions. Co alloy contents are 0 at %, 26.2 at % and 39.9 at %, respectively.

XRD analysis showed that as-plated deposits are amorphous and that the heat-treated samples have their structure changed to crystalline. As an example, Figure 2 shows X-ray patterns of deposits obtained from NiCoP100 solution at 30 mA $cm^{-2}$, before and after heat treatment. Only one broad peak can be clearly seen in the spectrum of the sample before heat treatment, indicating an amorphous structure. On the other hand, after heat treatment, the sample shows a typical spectrum of a crystalline structure.

Potentiostatic anodic curves were obtained in the NaCl 0.1 M solution for samples from all the conditions showed in Table 1. The effects of deposition current density on the anodic behaviour of Ni–P alloys are seen in Figure 3. In the range studied, no significant influence on the polarization curves can be observed. The same behaviour was also verified for Ni–Co–P alloy deposits produced in the solutions with both $Co^{2+}$ concentrations. Figure 4 displays an example of the effects of electrolyte composition on the anodic behaviour of alloy deposits obtained at 120 mA $cm^{-2}$. For the sample obtained in the NiP electrolyte, a current plateau is observed. This can be associated with a passivation process [1, 2–9, 14]. The constant current value extends from −100 mV to +200 mV and is followed by an increase in the current with anodic polarization. A similar behaviour was detected for deposits produced in the electrolytes with addition of $Co^{2+}$. In this case, however, the current plateau is broader and ranges, in average, from −180 to +300 mV. Additionally, the current value of the plateau decreases with increasing Co content in the deposit, as can be seen in the same Figure 4. This behaviour indicates that the presence of Co in the alloy deposits provides better corrosion performance in the medium studied. Since it was not observed any pitting at the end of the tests, one can

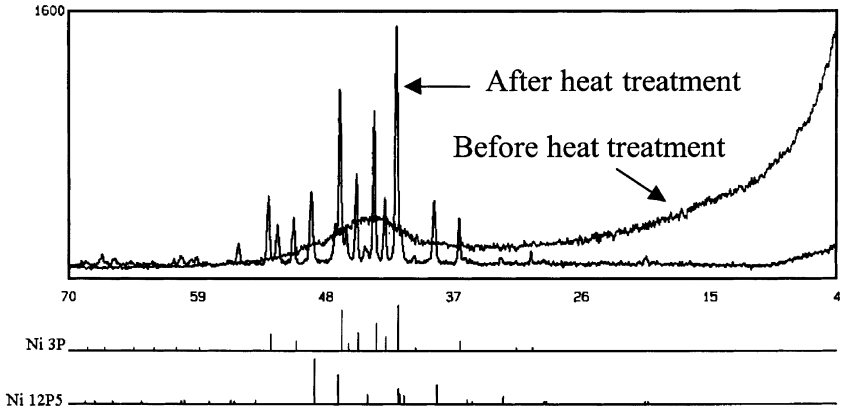


*Fig. 2.* X-ray diffraction spectra of Ni–Co–P alloys obtained at 30 mA $cm^{-2}$ in the solution with 100 g $l^{-1}$ $Co^{2+}$, before and after heat treatment.

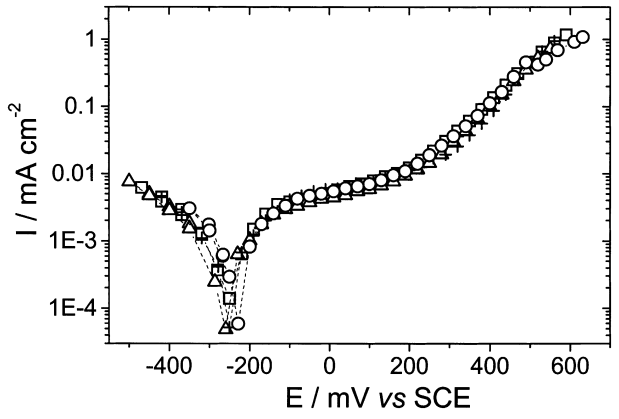


*Fig. 3.* Polarization curves in NaCl 0.1 M solution of Ni–P alloy deposits obtained at different current densities: (□) 30, (△) 60, (+) 90 and (○) 120 mA $cm^{-2}$.

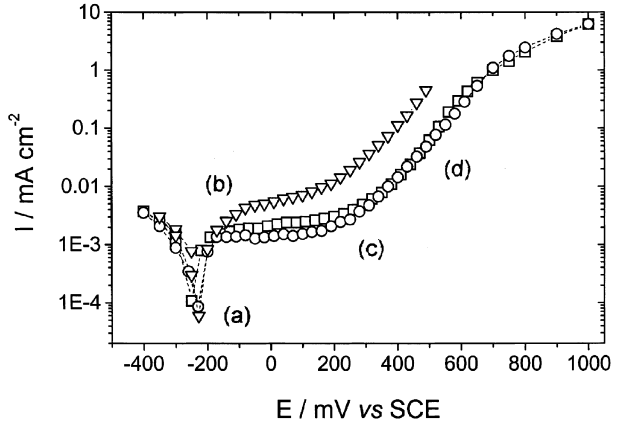


*Fig. 4.* Effects on polarization curves in NaCl 0.1 M of Co content in the alloy deposits obtained at 120 mA $cm^{-2}$ from (△) NiP, (□) NiCoP50 and (○) NiCoP100 solutions. The respective Co contents are: 0, 26.2 and 39.9 at %. (Marked regions for impedance measurements.)

suggest dissolution through the passive film (transpassivity) for all samples polarized to high anodic values, $E > +400$ mV.

The corrosion behaviour of Ni–P and Ni–Co–P alloys is clearly modified by the structural transition introduced by heat treatment. Figure 5 summarizes such behaviour. From the polarization curves of Ni–P

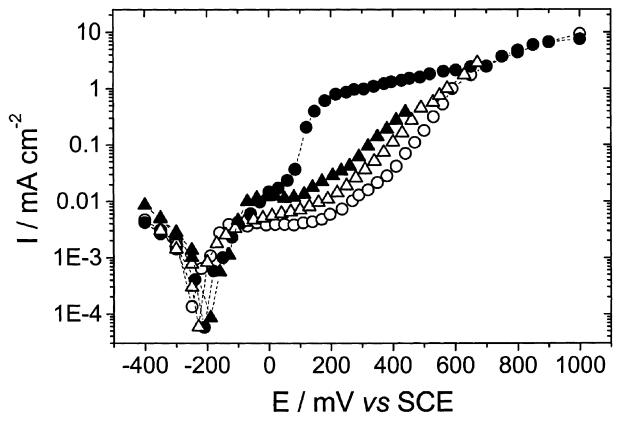


*Fig. 5.* Effects of the structure of Ni–P and Ni–Co–P (from NiCoP100 electrolyte) alloy deposits obtained at 120 mA $cm^{-2}$ on the polarization behaviour in NaCl 0.1 M. Ni–P amorphous (△) and crystalline (▲); Ni–Co–P amorphous (○) and crystalline (●).

samples obtained at 120 mA $cm^{-2}$, it was found that the passivation plateau is narrower and with a higher current value for the heat-treated sample. It is also possible to observe that the plateau practically disappears for the crystalline Ni–Co–P alloy and a steady current increase can be noted with increasing polarization. This result points to the fact that the structural state of the alloys is of primary importance as far as the ability of passivation is concerned.

Detailed information about the passivation behaviour of Ni–P and Ni–Co–P alloys was drawn from impedance data. Impedance measurements were performed at the regions marked on the polarization curves in Figure 4: at corrosion potential (a), at anodic potentials corresponding to the beginning (b) and to the end (c) of the current plateau and to the region of transpassivity (d). The results related to amorphous Ni–P and Ni–Co–P as well as crystalline deposits are shown, respectively, on Figures 6, 7 and 8. As a general remark, impedance ranges in Figure 6 (amorphous Ni–P samples) are smaller than in Figure 7 (amorphous Ni–Co–P samples), whereas both figures present ranges greater than those in Figure 8 (crystalline samples). In agreement with the polarization curves (Figures 4 and 5), this fact shows that the corrosion resistance of deposits is

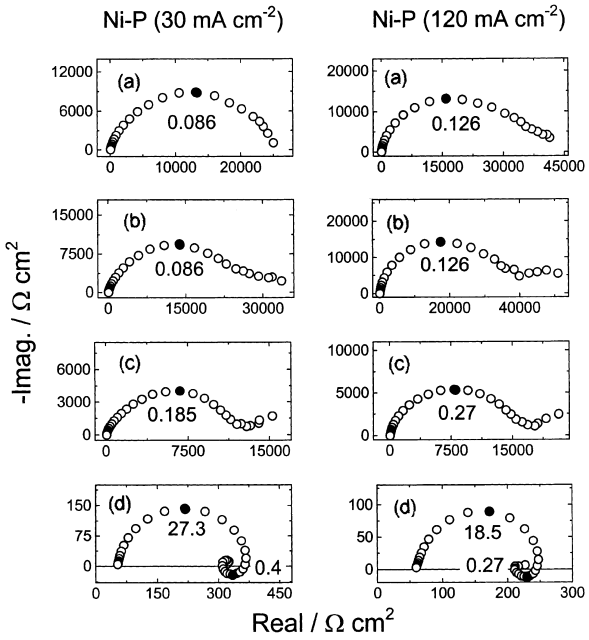


*Fig. 6*. Impedance diagrams obtained at the marked regions on Figure 4 for Ni–P amorphous samples obtained at 30 and 120 mA $cm^{-2}$ (frequencies in hertz).

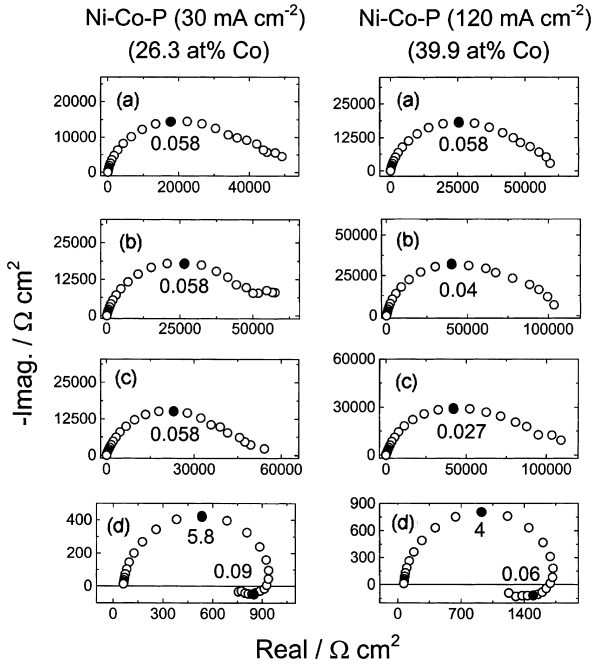


*Fig. 7*. Impedance diagrams obtained at the marked regions on Figure 4 for Ni–Co–P amorphous samples produced at 30 (26.3 at % Co) and 120 mA $cm^{-2}$ (39.9 at % Co) from NiCoP100 solution (frequencies in hertz).

improved by the amorphous condition and by the presence of alloying Co.

At the corrosion potential, diagrams (a), it is observed at least one capacitive loop for both samples in Figures 6, 7 and 8. It can be also noted a tendency of increasing the total impedance with increasing deposition current density. The impedance plots at the beginning of the current plateau, diagrams (b) present similar shape in

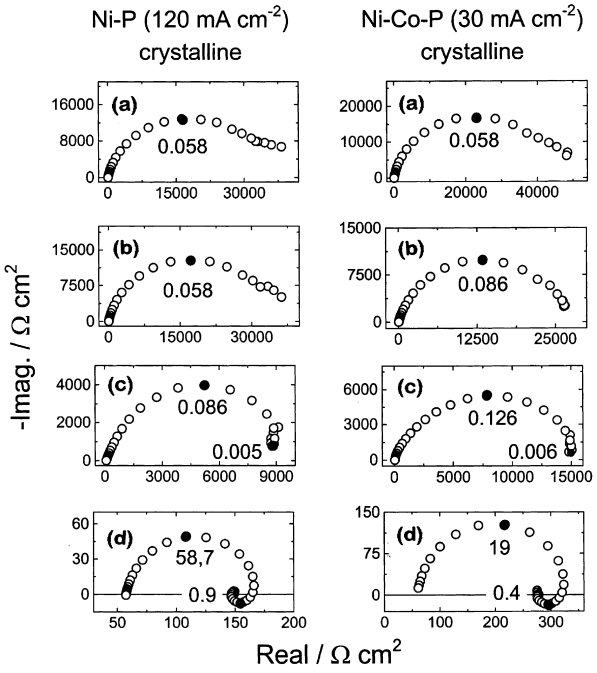


*Fig. 8*. Impedance diagrams obtained at the marked regions for Ni–P (120 mA $cm^{-2}$) and Ni–Co–P (30 mA $cm^{-2}$, solution NiCoP100) samples after heat treatment (frequencies in hertz).

the three Figures, suggesting the same kinetics of the dissolution–passivation process. In the case of the Ni–P diagrams (b) in Figure 6, no significant changes can be seen, as compared to those obtained at corrosion potential (diagrams (a)). However, Ni–Co–P alloys, diagrams (b) in Figure 7, depict increasing total impedance with increasing Co content. This result could be associated with a more efficient passivation process as a consequence of high Co content in the alloy. On the other hand, for crystalline samples there is a trend of decreasing total impedance values with increasing anodic potential, particularly for the Ni–Co–P sample, diagrams (b) in Figure 8.

At the end of the current plateau, diagrams (c) in Figure 6, there is a significant decrease on impedance values for Ni–P samples, if compared to the beginning of the plateau (diagrams (b)). This suggests that the passive film is no longer of protective nature. For Ni–Co–P, diagrams (c) in Figure 7, the behaviour is practically unchanged. Moreover, the higher the Co content in the alloy the higher the impedance. This fact confirms the better passivation process once Co is added to the alloy. Impedance plots obtained for Ni–P and Ni–Co–P crystalline samples, at the end of the plateau, diagrams (c) in Figure 8, differ significantly from those taken at its beginning, diagrams (b). Indeed, smaller impedance values are verified and an additional low frequency loop appears. These findings confirm the poor passivation process of the crystalline alloy deposits.

Finally, impedance plots obtained in the region of transpassivity, diagrams (d), are typical of a dissolution process for all samples. They show a capacitive loop whose capacitance corresponds to the double layer value

($\sim$20 $\mu$F cm$^{-2}$), followed by an inductive loop in the low frequency domain. Taking into account the charge transfer resistance values ($R_t$) associated with this loop, it can be noted that the dissolution process is more intense for the Ni–P (Figure 6) than for the Ni–Co–P (Figure 7) amorphous alloys. Crystalline samples also show low values of $R_t$, especially for the Ni–Co–P sample, which indicates a faster dissolution process (Figure 8). This confirms the crucial role of the structural state of the alloy in agreement with other authors [2, 3, 9].

Total immersion tests monitored by impedance measurements give additional information on the corrosion kinetics of Ni–P and Ni–Co–P alloys. Figure 9 shows the relationship between polarization resistance ($R_p$), taken from the impedance plots, and the immersion time for Ni–P ((a) and (b)), as well as for Ni–Co–P alloy samples ((c) and (d)). Comparing the two kinds of alloys obtained at the same deposition current density, it is seen that Ni–Co–P deposits always have higher $R_p$ values. This confirms the better corrosion performance of Ni–Co–P. Moreover, Ni–P samples presented red corrosion around 10 days of immersion whereas Ni–Co–P showed red spots only after 25–40 days.

Another interesting feature that can be observed in Figure 9 is the presence of a transition on the behaviour of all samples by the end of the first day of immersion. At the beginning of immersion, $R_p$ increases with immersion time, as seen in Figure 9(e). This becomes more intense, with increasing Co content in the alloy. After this period, there is an abrupt decrease in the $R_p$ values, which remain approximately constant until corrosion spots appear. It should be noted, however, that the final values

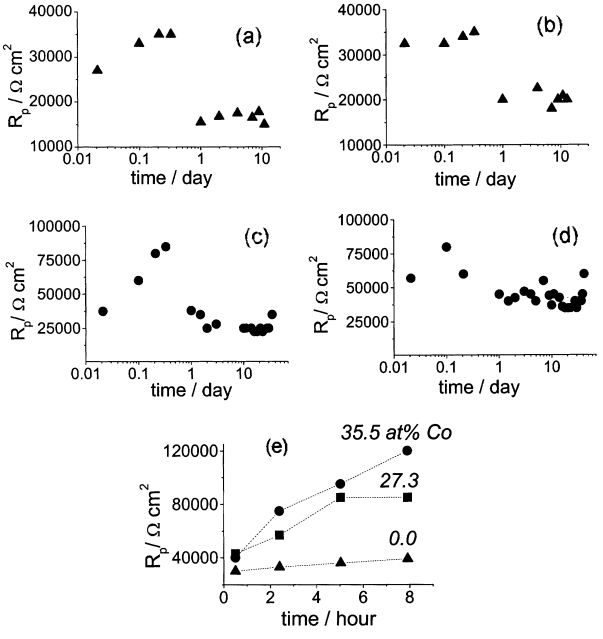


*Fig. 9.* Polarization resistance ($R_p$) against immersion time in NaCl 0.1 M: Ni–P alloy samples obtained at (a) 30 and (b) 120 mA cm$^{-2}$; Ni–Co–P samples obtained at (c) 30 and (d) 120 mA cm$^{-2}$ from NiCoP100 solution; (e) behaviour of samples obtained at 90 mA cm$^{-2}$ from the three different electrolytes at the beginning of immersion: NiP (▲), NiCoP50 (■) and NiCoP100 (●).

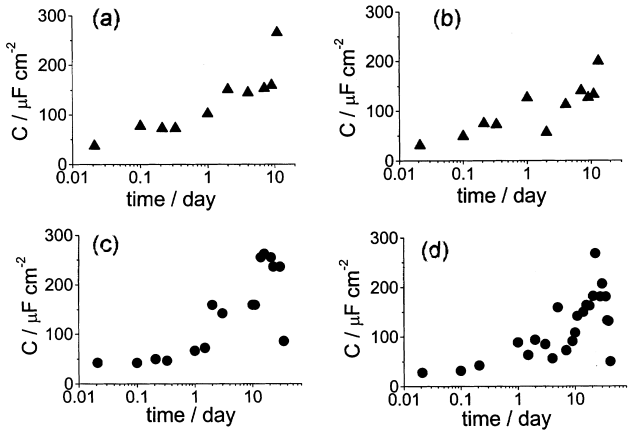


*Fig. 10.* Capacitance ($C$) against immersion time in NaCl 0.1 M: Ni–P alloy samples obtained at (a) 30 and (b) 120 mA cm$^{-2}$; Ni–Co–P obtained at (c) 30 and (d) 120 mA cm$^{-2}$ from NiCoP100 electrolyte.

of $R_p$ are higher the greater the Co content in the alloy. These findings suggest the existence of two different dissolution mechanisms occurring on both kind of alloys. Crousier et al. [8] proposed that Ni–P deposits have a layered structure, where two different alloys with different P contents exist. The dissolution mechanism for both Ni–P and Ni–Co–P alloy deposits may be related to these heterogeneous structures.

An apparent transition behaviour can also be seen in Figure 10. The capacitance against immersion time plots display a change of slope at the end of the first day of immersion. This corroborates the findings in Figure 9 and points to a possible two step dissolution mechanism of both Ni–P and Ni–Co–P alloys.

## 4. Conclusions

The results show that the Co content in alloy deposits increases with deposition current density and $Co^{2+}$ concentration in solution. No obvious relationship between P content in the deposits and these studied parameters was observed. Both Ni–P and Ni–Co–P alloys were found to have amorphous structure, with P content in the range of 14–20 at %. Heat treatment at 500 °C in $N_2$ atmosphere for 1 h caused crystallization of these alloys.

Polarization curves in NaCl 0.1 M revealed that both Ni–P and Ni–Co–P amorphous alloys show a current plateau, associated with a passive film formation at the alloy surface. This passivation process is strongly affected by Co content. As the Co content in the deposit is increased, the plateau is broadened and the current values decrease. This suggests a more efficient passivation process on Ni–Co–P alloys. Structural modification produced by heat treatment also affected this behaviour. For Ni–P alloys, the crystalline structure resulted in a shift of the curves to higher current values. Moreover, in Ni–Co–P crystalline alloys, an increase in Co content tends to eliminate the plateau, suggesting the nonprotective nature of the passive film.

Impedance measurements permitted a more detailed characterization of the corrosion behaviour of Ni–P and Ni–Co–P alloys. The impedance diagrams obtained at the corrosion potential suggested a better corrosion performance of amorphous alloys produced with increasing deposition current density and increasing $Co^{2+}$ concentration in the solution. Comparing amorphous and crystalline samples, no differentiation was observed on the impedance diagrams at the corrosion potential. Measurements performed with anodic polarization showed a marked difference in the passivation process. For higher alloy Co content, the impedance diagrams at the end of the plateau suggested a better resistance of the passive film. Furthermore, crystalline samples presented a change in impedance plots at high polarization, characterized by the appearance of an inductive feature. This confirms the role of the structural condition of the alloy. Additionally, total immersion tests suggested the existence of a two step dissolution mechanism for both Ni–P and Ni–Co–P alloys.

## Acknowledgements

The authors wish to thank the financial support of the following Brazilian agencies: CNPq, FUNCAP, FUJB and FAPERJ.

## References

1. J.L. Carbajal and R.E. White, *J. Electrochem. Soc.* **135** (1988) 2952.
2. A. Królikowski and P. Butkiewicz, *Electrochim. Acta* **38** (1993) 1979.
3. P. Lima Neto, F.J.B. Rabelo, A.M.M. Adam, E.R. Gonzalez and L.A. Avaca, *Química Nova* **19** (1996) 345.
4. A. Budniok and P. Matyja, *Thin Solid Films* **201** (1991) 305.
5. T. Morikawa, T. Nakade, M. Yokoi, Y. Fukumoto and C. Iwakura, *Electrochim. Acta* **42** (1997) 115.
6. E. Bredael, B. Blanpain, J.P. Celis and J.R. Roos, *J. Electrochem. Soc.* **141** (1994) 294.
7. A.S.M.A. Haseeb, P. Chakraborty, I. Ahmed, F. Caccavale and R. Bertoncello, *Thin Solid Films* **283** (1996) 140.
8. J. Crousier, Z. Hanane and J.-P. Crousier, *Thin Solid Films* **248** (1994) 51.
9. P.-H. Lo, W.-T. Tsai, J.-T. Lee and M.-P. Hung, *Surf. Coat. Technol.* **67** (1994) 27.
10. N. Fenineche, A.M. Chaze and C. Coddet, *Surf. Coat. Technol.* **88** (1997) 264.
11. J. Bielinski, A. Królikowski, I. Kedzierska and W. Stokarski, *ACH-Models in Chem.* **132** (1995) 685.
12. H. Habazaki, S.-Q. Ding, A. Kawashima, K. Asami, K. Hashimoto, A. Inoue and T. Masumoto, *Corros. Sci.* **29** (1989) 1319.
13. S.J. Splinter, R. Rofagha, N.S. McIntyre and U. Erb, *Surf. Interf. Anal.* **24** (1996) 181.
14. R.B. Diegle, N.R. Sorensen, C.R. Clayton, M.A. Helfand and Y.C. Yu, *J. Electrochem. Soc.* **135** (1988) 1085.
15. M.A. Helfand, C.R. Clayton, R.B. Diegle, N.R. Sorensen and Y.C. Yu, *J. Electrochem. Soc.* **139** (1992) 2121.